Applied Catalysis B: Environmental 105 (2011) 211–219

Contents lists available at ScienceDirect

Applied Catalysis B: Environmental

journal homepage: www.elsevier.com/locate/apcatb

Room-temperature synthesis of single-crystalline Se nanorods with remarkable photocatalytic properties

Yao-De Chiou, Yung-Jung Hsu*

Department of Materials Science and Engineering, National Chiao Tung University, 1001 University Road, Hsinchu 30010, Taiwan, ROC

ARTICLE INFO

Article history:
Received 28 January 2011
Received in revised form 31 March 2011
Accepted 12 April 2011
Available online 20 April 2011

Keywords:
Selenium
Nanorods
Photocatalysis
Memory effect
Carboxylmethyl cellulose

ABSTRACT

We demonstrated for the first time that single-crystalline Se nanorods (NRs), prepared with a facile chemical reduction approach at room temperature, may display noticeable catalytic activities toward methylene blue degradation in dark environment after subjected to a short period of irradiation. Such capability of photocatalysis in the dark for Se NRs was attributed to the memory effect related to pre-irradiation treatment. The result of spin-trapping electron paramagnetic resonance measurement suggests that a sustained supply of •OH radicals could be attained for Se NRs upon the cease of irradiation, which is accountable for the memory photocatalytic effect as revealed in the dark. As compared to the commercial P-25 TiO_2 powder and Se nanoparticles, the as-synthesized Se NRs exhibited superior photocatalytic performance under UV illumination, demonstrating their potential as active photocatalysts in relevant redox reactions. Furthermore, the recycling test reveals that Se NRs could be promisingly utilized in the long-term course of photocatalysis. The present Se NRs may find potential use for unique photocatalytic applications, in which typical photocatalysis prevails under light illumination, while memory photocatalytic effect takes over when irradiation is interrupted.

1. Introduction

Elemental selenium (Se) possesses many unique physical and chemical properties, which makes it a fascinating material in relevant optoelectronic and physicochemical applications. For instance, its noticeable photoconductivity (8×10^4 S cm^{-1}) offers great potential in the fields of solar cells, rectifiers, photographic exposure meters, xerography and solid-state light sensing [1,2]. The catalytic activities of Se toward hydration and oxidation reactions suggest that Se might be a promising catalyst in chemical synthesis [3,4]. In addition, Se exhibits high reactivity to a variety of chemicals, which can be exploited to directly convert it into other functional materials like Ag_2Se [5–9], CdSe [10], PbSe [11], $NiSe_2$ [11], $RuSe_2$ [12], $Pd_{17}Se_{15}$ [12], CuAgSe [13], and Pt [14,15]. In the past decade, considerable efforts have been devoted to the preparation of Se nanostructures to further the development of Se.

Among the various nanostructures, one-dimensional (1-D) nanocrystals including nanowires, nanorods and nanotubes are of particular importance since they have been proven effective in a wide range of applications [16–19]. Over the past few years, many liquid-phase synthetic strategies were developed to produce 1-D Se nanocrystals with controllable dimensions, for example, the sonochemical approach [20–24], the self-seeding process [3,25–29], the hydrothermal method [4,30–32], the photothermally-assisted technique [33], and the micelle-mediated synthesis [34]. Most of the above synthetic routes to 1-D Se nanocrystals are characteristic of elaborate reaction conditions such as the intense ultrasonication [20–24], the long aging process [3,25–28], the elevated reaction pressure and temperature [4,30–32], as well as the use of harmful chemicals like hydrazine [20–23,25,33] and surfactant [32,34]. Such need of complicated procedures may further hinder the applicability of Se. Therefore, creation of a more facile, mild synthetic approach from which one can obtain 1-D Se nanocrystals with controllable dimensions is crucial to their practical applications.

In this work, we developed a facile chemical reduction approach to prepare single-crystalline Se nanorods (NRs) at room temperature. The synthesis used commercially available SeO_2 powder as the precursor, relatively environmentally friendly $NaBH_4$ as the reducing agent, and a biocompatible polysaccharide as the morphology-directing agent. The formation of Se NRs involved the reduction of H_2SeO_3 with $NaBH_4$ to form Se particle seeds, followed by the anisotropic crystal growth of Se directed by polysaccharide molecules and the subsequent crystal growth along a preferred direction from these seeds to form NRs. We analyzed various aspects of the synthetic approach, discussed the photocatalytic properties of products, and demonstrated for the first time that Se NRs may display noticeable photocatalytic activities in dark environment after subjected to a short period of irradiation. The result of spin-trapping electron paramagnetic resonance (EPR) measurement suggests that a sustained supply of •OH radicals could be

* Corresponding author. Tel.: +886 3 5712121x55317; fax: +886 3 5724724.
E-mail address: yhsu@cc.nctu.edu.tw (Y.-J. Hsu).

0926-3373/$ – see front matter © 2011 Elsevier B.V. All rights reserved.
doi:10.1016/j.apcatb.2011.04.019

attained for Se NRs upon the cease of irradiation, which is accountable for the memory photocatalytic effect as revealed in the dark. As compared to the commercial P-25 TiO_2 powder and Se nanoparticles, the as-synthesized Se NRs exhibited superior photocatalytic performance toward methylene blue photodegradation, demonstrating their potential as an active photocatalyst in relevant redox reactions. Moreover, no appreciable decay of photocatalytic efficiency was found for Se NRs after repeated uses and recycled, revealing their promising potential in the long-term course of photocatalysis.

2. Experimental

2.1. Chemicals

All chemicals were analytic grade reagents and used without further purification.

2.2. Preparation of Se NRs

The synthesis of Se NRs was carried out in a chemical reduction process. In the typical procedure, sodium salt of carboxymethyl cellulose (denoted as CMC, M_w = 90,000 Da, 4.0 wt.%) was dissolved in deionzed water (9.0 mL) at room temperature, followed by the addition of NaOH solution (1.0 mL, 1.0 M) and SeO_2 powder of a given amount (0.111 g, 1.0 mmol). Note that selenious acid (H_2SeO_3) was formed when SeO_2 was dissolved in aqueous solution. The mixed solution was then stirred vigorously at room temperature until it became transparent, producing the CMC-stabilized H_2SeO_3 solution. Subsequently, $NaBH_4$ solution (1.0 mL, 1.0 M) was added dropwise to the CMC-stabilized H_2SeO_3 to carry out the reduction reaction. After stirring at 25 °C for 2 h, brown suspending solids were produced in the reaction solution. The resultant brown precipitate (Se NRs) was collected by centrifugation at 10,000 rpm for 10 min and washed with distilled water and ethanol to remove remaining ions and impurities. The product was then dried and stored at 60 °C in vacuum for later use. In this work, reduction reaction was carried out at different temperatures (25, 50 and 100 °C) to investigate the effect of reaction temperature on the morphology of the resulting Se. Besides, experiment using poly(vinylpyrrolidone) (PVP, M_w = 29,000 Da, 4.0 wt.%) as the soft-template was also conducted to compare with the result using CMC

2.3. Dimension control for Se NRs

To produce NRs with different aspect ratios, various amounts of NaOH (from 0 to 1.2 mmol) added in the CMC solution were employed. The pH value of CMC solution upon the addition of NaOH of 0, 0.3, 0.6, 0.9, 1.0, and 1.2 mmol was 3.8, 4.0, 4.9, 7.9, 8.2, and 11.5, respectively. The product obtained with the addition of NaOH of 0, 0.3, 0.6 and 0.9 mmol was denoted as Se NP, Se NR-1, Se NR-2 and Se NR-3, respectively.

2.4. Spin-trapping EPR measurement

The sample for EPR measurement was prepared by mixing Se NRs of fixed amount (0.1 mg) with the spin-trapping reagent (5,5-dimethyl-1-pyroline-*N*-oxide, denoted as DMPO, 0.01 M) in an aerated aqueous solution (1.0 mL). A high-pressure mercury lamp (400 W) was used to irradiate the sample. The EPR spectrum of DMPO–•OH adducts was first obtained from sample under continuous irradiation for 5 min. The illumination was then switched off, and the signals were recorded in situ to monitor the variation of EPR spectrum with time. To quantitatively analyze the decay process of DMPO–•OH adducts, the double integrated peak areas of EPR spectra were calculated and represented [35–37].

2.5. Photocatalytic performance measurement

The photocatalytic performance of Se NRs was evaluated by the photodegradation of methylene blue (denoted as MB) under UV illumination. A quartz tube with a capacity of 30 mL was used as the photoreactor vessel. The optical system used for photocatalytic reaction was composed of a UV lamp (8 W) with a light intensity of 3.5 mW/cm^2. All the photocatalysis experiments were conducted at room temperature. Five kinds of photocatalysts including three Se NR samples (Se NR-1, Se NR-2, Se NR-3), Se nanoparticles (Se NP) and Degussa P-25 TiO_2 powder were used and compared in the photodegradation of MB. In a typical experiment, 10 mg of photocatalyst was added into 20 mL of MB solution (1×10^{-5} M) in the photoreactor vessel. Prior to irradiation, the suspension was stirred in the dark for 60 min to reach the adsorption equilibrium between MB and photocatalyst. At certain time intervals of irradiation, 1.0 mL of the reaction solution was withdrawn and centrifuged to remove the photocatalyst particles. The filtrates were analyzed with a UV–vis spectrophotometer to measure the concentration variation of MB through recording the corresponding absorbance of the characteristic peak at 665 nm. To investigate the reusability and stability of photocatalyst, four cycles of photocatalytic reactions were conducted by using Se NR-1 as the representative sample.

2.6. Characterization

The morphology and dimensions of the products were examined with a field-emission scanning electron microscope (FESEM, Jeol, JSM-6500F). The compositional information was obtained with the X-ray photoelectron spectroscope (XPS, VG Scientific, Microlab 350) using Mg Kα ($h\nu$ = 1253.6 eV) as X-ray source under a base pressure of 1.0×10^{-9} Torr. All the binding energies were calibrated by C1 s at 284.6 eV. The deconvolution of O1s XPS spectra for the samples was performed using XPSPEAK software with 20% Lorentzian and 80% Gaussian peak feature set for the fitting. The crystallographic structure of the samples was investigated with X-ray diffraction (XRD, MAC Science, MXP18) and a high-resolution transmission electron microscope (HRTEM, JEOL, JEM-2100) operated at 200 kV. The viscosity of CMC solution was measured with the Brookfield DV-III Ultra Rheometer in steady shear mode (shear rate = 3.7 s^{-1}). UV–vis absorption spectra were obtained using a Hitachi U-3900H spectrophotometer at room temperature. Brunauer–Emmett–Teller (BET) surface area of the samples was estimated from the N_2 adsorption/desorption analysis. X-band EPR spectra in first-derivative presentation for •OH radicals spin-trapped by DMPO were recorded using a Bruker Elexsys E-580 spectrometer. The typical settings of EPR measurement were 3480 G for center field, 100 G for sweep width, 9.76 GHz for microwave frequency, and 1.5 mW for microwave power

3. Results and discussion

3.1. Structural investigation

The redox potentials for SeO_3^{2-}/Se and BH_4^-/$B(OH)_3$ couples are 0.74 and 0.48 V versus NHE, respectively [38,39]. Reduction of H_2SeO_3 with $NaBH_4$ would thus spontaneously occur to generate elemental Se at room temperature. In the current work, reduction reaction of CMC-stabilized H_2SeO_3 using $NaBH_4$ at 25 °C for 2 h produced NRs with considerably uniform dimensions. As shown in Fig. 1a, these NRs had a typical diameter of 40–60 nm and length up to 1 μm. The compositional information of NRs was then studied with XPS and XRD. Fig. 1b shows the XPS spectrum of Se 3d

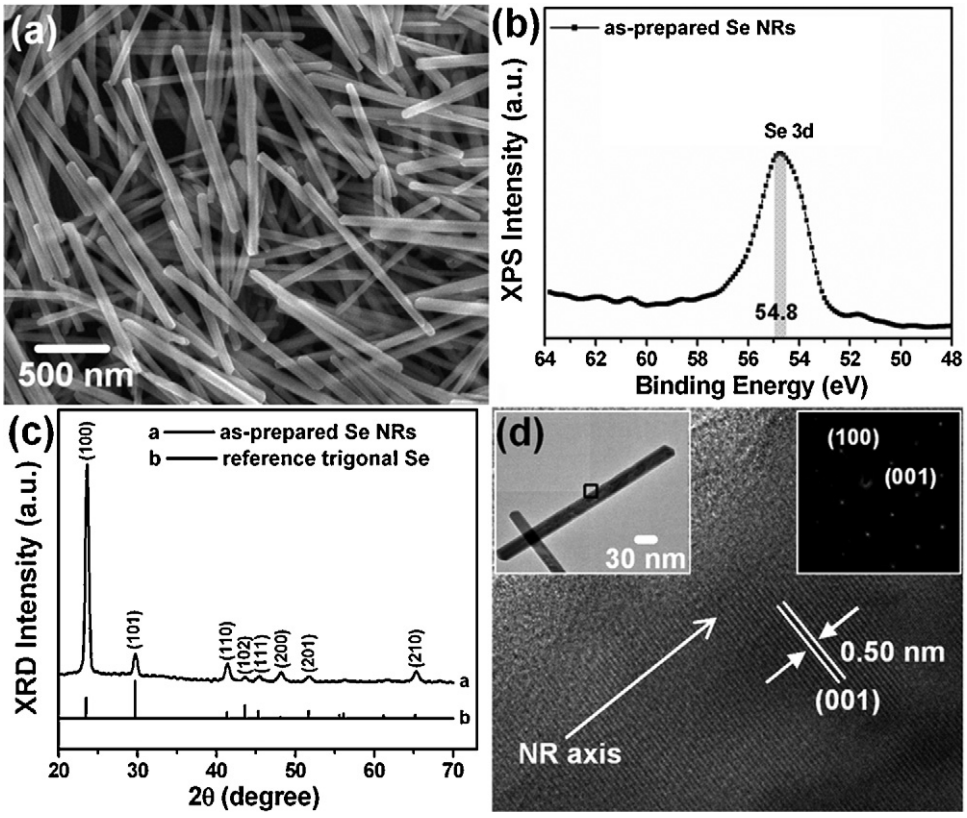

Fig. 1. (a) SEM image, (b) XPS Se 3d spectrum, (c) XRD pattern, and (d) HRTEM analysis for the as-synthesized Se NRs. (c) The pattern of reference trigonal Se (JCPDS 06-0362) was also included for comparison. The amount of NaOH added was 1.0 mmol.

for the as-synthesized NRs. The binding energy observed at 54.8 eV corresponded well to the Se 3d doublets of elemental Se [40], implying that the as-obtained NRs were made of Se. The corresponding XRD pattern shown in Fig. 1c confirms the formation of trigonal Se. We noticed that a relatively intense (1 0 0) peak as compared to the standard pattern was recorded, indicating a preferred growth direction of [0 0 1] in Se NRs [3,22,30,31]. In addition, there were no diffraction peaks attributable to SeO_2 or other impurities, demonstrating the success of the current process for production of pure Se. Fig. 1d further shows the detailed crystallographic structure of the as-prepared Se NRs. The dot pattern of the inserted selected area electron diffraction (SAED) image suggests the single crystallinity of the NR product. The lattice image taken on an individual NR clearly reveals the (0 0 1) lattice plane of trigonal Se with a *d* spacing of 0.50 nm. Furthermore, the axis of the NR was found to be parallel to the [0 0 1] direction, implying that Se NRs were grown along the [0 0 1] direction, which is consistent with the indication from XRD. This result, together with those of XPS, XRD and SAED analyses, confirms the formation of single-crystalline Se NRs at 25 °C by reducing H_2SeO_3 with $NaBH_4$ in the presence of CMC.

3.2. Growth mechanism

The growth mechanism for 1-D Se nanocrystals in solution-based approaches has been extensively studied in literature [20–29]. In general, there are three steps involved in the liquid-phase growth of 1-D Se. At first, precursor of Se is decomposed with suitable reagent to form amorphous Se particles. Subsequently, seeds of trigonal Se are generated provided that a definite driving force, such as the ultrasonication operation [20,21,23,24] or the abrupt cooling/aging treatment [3,25,26,28], is applied. Finally, anisotropic crystal growth occurs to build 1-D nanoarchitecture from these seeds, accompanied by the re-dissolution of the first-formed amorphous Se particles. The above mechanism however could not explain the formation of Se NRs in this work because we did not observe the generation of amorphous Se and no extra driving force was provided. To comprehend the formation process for the present NRs, their morphological evolution was investigated by conducting experiments with various reaction times. As displayed in Fig. 2, Se particles of 40–50 nm in size were first generated at the early stage of reaction. Note that these particles were crystalline and also possessed the crystal structure of trigonal Se, as verified by the SAED analysis (data not shown here). Some particles then grew adjacently to each other to form warm-like particle aggregations. Afterward branched structures grew out of both the particle aggregations and the individual particles to evolve the 1-D architecture of Se. Continued longitudinal growth in these quarsi-1-D structures eventually led to the formation of NRs with uniform dimensions.

A plausible growth mechanism for the present Se NRs was proposed and illustrated in Fig. 2g. In the CMC-stabilized H_2SeO_3 solution, selenious ions (SeO_3^{2-}) were believed to distribute along the molecular chains of CMC through binding to CMC's OH groups. It has been pointed out that SeO_3^{2-} may substitute the hydrogen of OH groups of polysaccharide molecules [41], which can be revealed with the corresponding XPS analysis. Fig. 3 compares the XPS spectrum of O1s between pure CMC and CMC-stabilized H_2SeO_3 solutions. For the pure CMC sample, the O1s XPS peak at 531.1 eV (O1 component) represented the oxygen components typically found in polysaccharides [41]. As to the CMC-stabilized H_2SeO_3, an additional peak at the higher binding energy of 533.0 eV was observed (O2 component). Such higher binding energy of O1s in the CMC-stabilized H_2SeO_3 resulted from the replacement of the hydrogen of OH groups of CMC with the more electronegative Se=O of SeO_3^{2-} [41]. It is because of the binding of SeO_3^{2-} along the molecular chains of CMC that the adjacent growth among Se particles may proceed to evolve the 1-D architecture. After this stage, Se

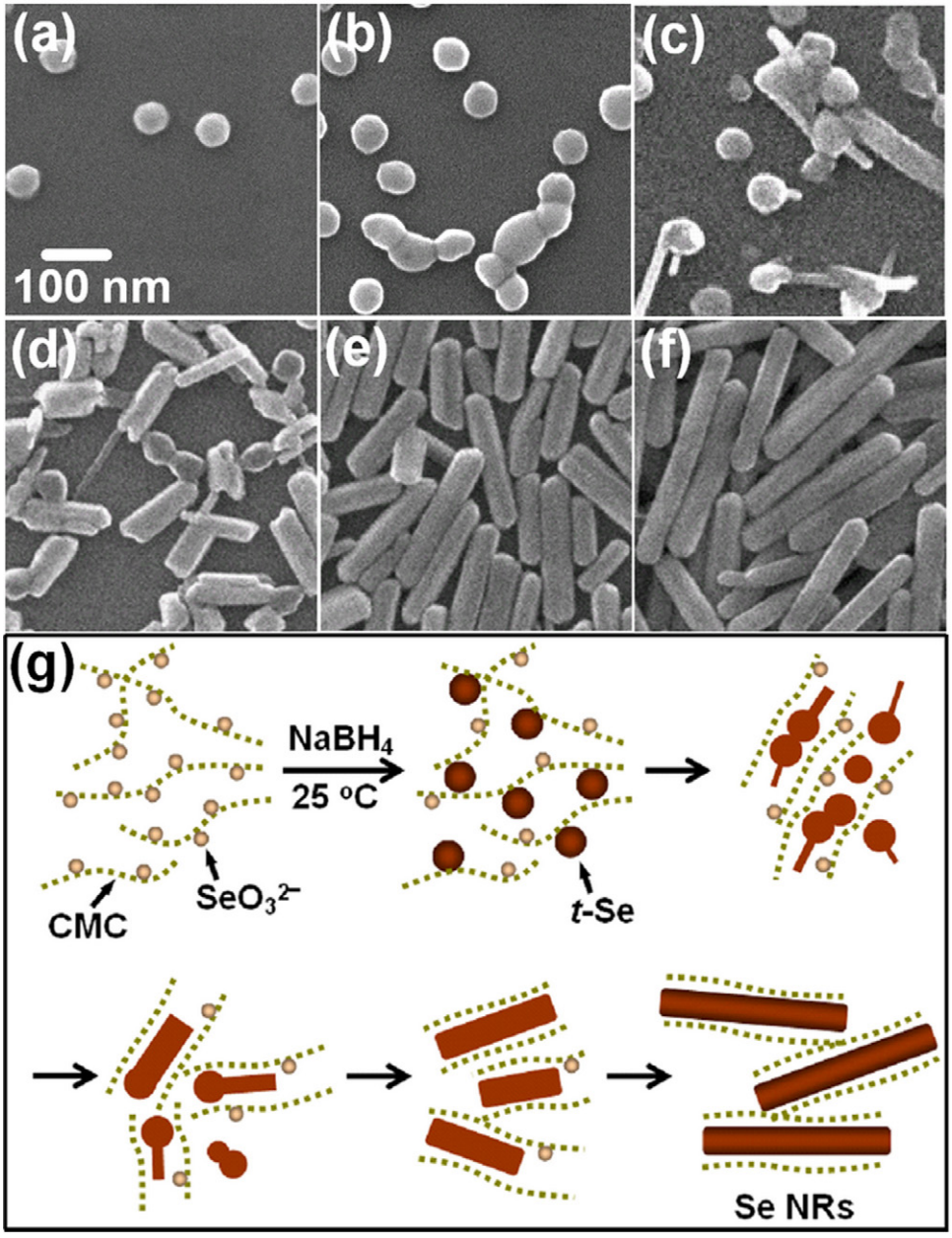

Fig. 2. SEM images of Se samples obtained at various reaction times: (a) 5 min, (b) 10 min, (c) 20 min, (d) 60 min, (e) 80 min, (f) 100 min. A schematic illustration of the growth mechanism for Se NRs was depicted in (g). The amount of NaOH added was 1.0 mmol.

tended to nucleate and grow at the surfaces of the particle aggregations and the first-formed particles, which can be inferred from the morphology observed at the reaction time of 20 min. Anisotropic growth then gradually dominated the crystal growth, enabling a predominant growth along the [0 0 1] of Se to lead to the formation of NRs. On the other hand, CMC molecules that surrounded the growing species also played an important role in the formation of Se NRs. As shown in Fig. 4a, reduction reaction of H_2SeO_3 in the absence of CMC only produced bulky particles with irregular morphology, which manifests that CMC molecules guided the NR growth through their binding to the specific crystal planes of Se. Note that CMC has been widely used as capping reagent to prepare a variety of nanocrystals such as Ag [42], Pt [43], Pd [44–46], Fe–Pd [47], and Co–Pt alloys [48]. It is generally believed that CMC could bind to the surfaces of the grown crystals, adjusting their growth rates to render the production of nanocrystals with controllable morphology. In this work, we suggested that CMC might attach to the {1 0 0} planes of Se and suppress the growth rates of these planes, while the {0 0 1} planes, covered with the least amount of CMC, grew the fastest to form NRs. The growth direction of [0 0 1] of Se NRs observed in the XRD and HRTEM analyses supported the above argument. Moreover, as we replaced CMC with PVP, a common stabilizer used for preparation of 1-D Se nanocrystals [28,33,49], in the chemical reduction process, particulate nanocrystals with non-uniform dimensions were obtained (Fig. 4b). This result reveals the indispensable role of CMC in the growth of uniform Se NRs from the current chemical reduction process.

3.3. Effects of reaction temperature and NaOH amount

In addition to the use of CMC, the reaction temperature and the amount of NaOH added influenced the morphology of the resulting Se as well. Fig. 4c and d displays the morphology of Se products obtained at 50 and 100 °C, respectively. When chemical reduction

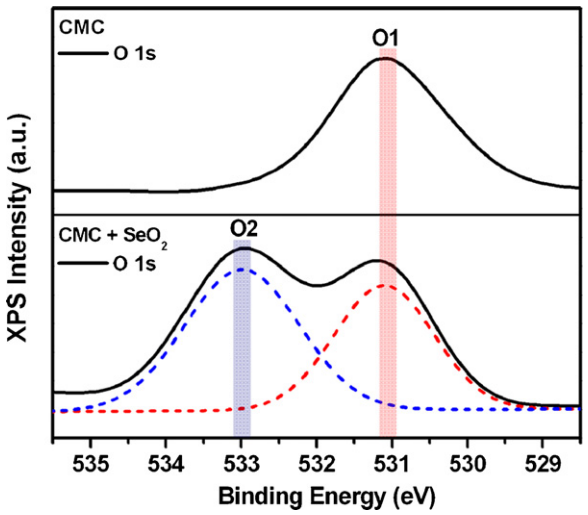

Fig. 3. XPS spectra of O1s for pure CMC and CMC-stabilized H_2SeO_3 solutions. The deconvoluted peaks were also included for comparison (dash lines).

was conducted at a higher temperature of 50 °C, bundles of Se NRs with thicker diameter (500–800 nm) and longer length (5–8 μm) were obtained. The extensive growth in the lateral and longitudinal dimensions of NRs was more pronounced as the reaction temperature was further elevated to 100 °C. The change in the conformation of CMC with temperature may account for such size variation in NR products observed. It has been reported that the viscosity of CMC decreased dramatically with increasing temperature [50]. For the CMC solution that contained NaOH of 1.0 mmol, the viscosity measured at 25, 50 and 100 °C was 53.4, 26.3, and 7.5 cp, respectively. Evidently, the elevation of reaction temperature to 50 and 100 °C resulted in a huge drop of viscosity for the current CMC solution, which may facilitate the diffusion and growth processes associated with NR formation [51,52]. As a consequence, NRs with larger dimensions and wider size distribution were formed at 50 and 100 °C. The dimensions of Se NRs can be further tuned by controlling the amount of NaOH added in the CMC solution. It should be noted that we failed to obtain NR product in the CMC-stabilized chemical reduction process without the addition of NaOH. This is mainly a result of the increasing reducing power of $NaBH_4$ at the relatively acid condition [53,54], which would accelerate the nucleation and growth of Se to promote isotropic crystal growth and therefore produce nanoparticles. With the addition of 0.3 mmol NaOH, NRs having the diameter of 40–60 nm and length of 180–220 nm (an average aspect ratio of 4.1) were formed. As increasing the amount of NaOH from 0.3 to 1.0 mmol, the length of the resulting NRs increased accordingly, corresponding to a raise in their aspect ratio from 4.1 to 19.7. Because the reducing power of $NaBH_4$ was depressed with increasing NaOH amount, the nucleation of Se would be progressively retarded to generate fewer Se seeds. The decreasing number of growing seeds at the early stage of reaction could eventually cause NR growth with increasing lengths [55]. Further increasing the NaOH amount to 1.2 mmol however led to the formation of NRs having comparable length (800 nm–1 μm) but thicker diameter (80–120 nm). This phenomenon could be accounted for by the combined effect of the varied conformation of CMC and the decreased reducing power of $NaBH_4$. As a polyelectrolyte, CMC solution is stable with a roughly constant viscosity over the pH range of 2–10, while a rapid decrease in its viscosity is observed at the pH value exceeding 10 [56,57]. In the current synthetic system, the pH value of CMC solution that contained NaOH of 1.0 and 1.2 mmol was 8.2 and 11.5, respectively, implying a lower viscosity for CMC when 1.2 mmol NaOH was added. Since the drop of viscosity for CMC with 1.2 mmol NaOH was apparent (from 58.8 cp for 1.0 mmol NaOH to 45.6 cp for 1.2 mmol NaOH), we believed that an effect similar to the elevated reaction temperature case would emerge to affect crystal growth and produce NRs with larger lateral dimensions. On the other hand, due to the significant

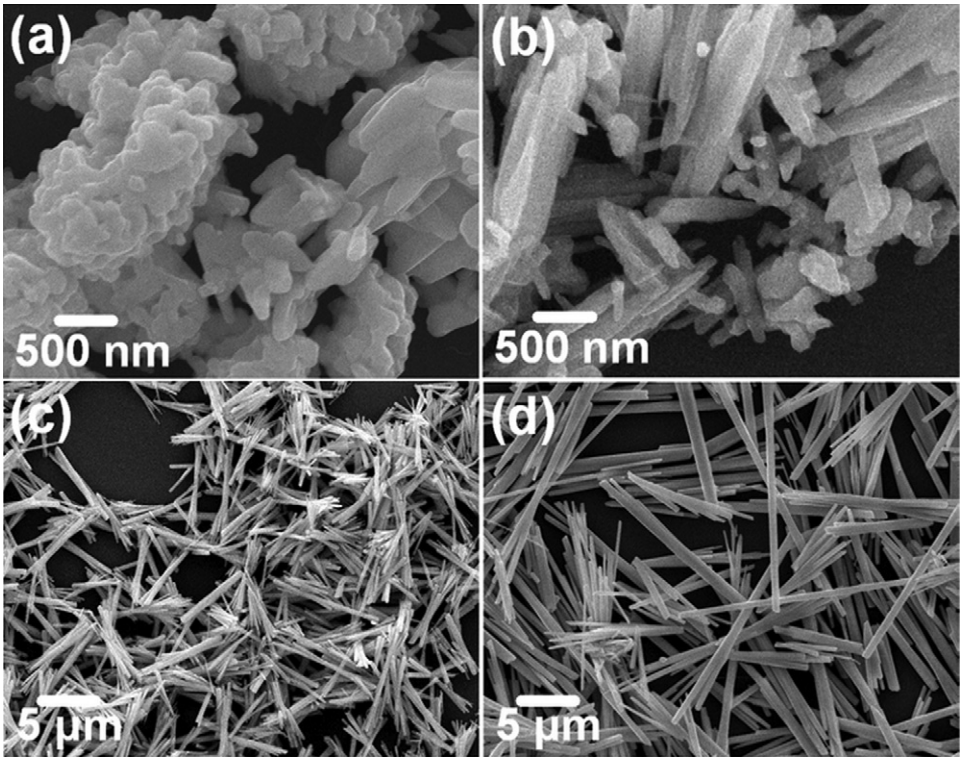

Fig. 4. SEM images of Se samples prepared with various reaction conditions: (a) without the use of CMC, (b) with the use of PVP, (c) at an elevated reaction temperature of 50 °C, (d) at an elevated reaction temperature of 100 °C. The amount of NaOH added was 1.0 mmol.

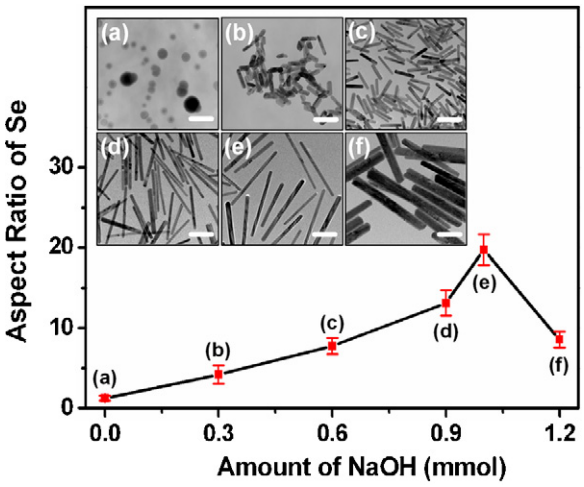

Fig. 5. Correlation of the aspect ratio of Se with the amount of NaOH added. Insets show the corresponding TEM images for Se samples and the scale bar is 200 nm.

depression in the reducing power of $NaBH_4$, the reduction reaction with NaOH of 1.2 mmol proceeded quite slowly. This retarded reaction progress may prohibit NRs from growing too long in a short reaction period (2 h), thus producing NRs having the length comparable to those obtained with NaOH of 1.0 mmol. For more clarity on the effect of NaOH addition, we depicted the correlation of the aspect ratio of Se with the amount of NaOH added in Fig. 5. In a short summary, the general trend observed here was that higher reaction temperature led to thicker and longer NRs, whereas larger NaOH amount (in the range of 0.3–1.0 mmol) gave longer NRs. By tuning these two parameters, Se NRs with controllable dimensions can be readily prepared.

3.4. Spin-trapping EPR spectra

Since Se is known for its remarkable photoconductivity, we surmised an intrinsically suppressed electron-hole recombination event during the charge transfer process for Se NRs [58–60]. This speculation can be confirmed by evaluating the light-energy conversion efficiency for Se NRs in their practical applications. Photocatalysis is a valuable approach for semiconductors to practically convert light into chemical energy. Experimental results have shown that reactive oxygen species such as $^{\bullet}O_2^-$ and $^{\bullet}$OH radicals are generated when adsorbed oxygen and water molecules scavenge the charge carriers of semiconductors. This course greatly affects the photocatalysis processes in aqueous suspensions of semiconductors. An examination of the formation of reactive radicals can thus provide useful information about the fate of charge carriers and lead to a greater understanding of photocatalysis for the present Se NRs. The spin-trapping EPR is an effective technique in identification of reactive radicals. Because $^{\bullet}$OH radicals are responsible for most of the photocatalysis processes in aqueous solutions, we collected EPR signals of $^{\bullet}$OH radicals spin-trapped by DMPO for Se NRs prepared in this work. Fig. 6a first illustrates the EPR spectra for Se NR-1 in the presence of DMPO under different experimental conditions. Under light illumination, four characteristic peaks of DMPO–$^{\bullet}$OH adducts with an intensity ratio of 1:2:2:1 were observed [61], demonstrating the production of $^{\bullet}$OH radicals in the irradiated suspension of Se NR-1. To comprehend the fate of $^{\bullet}$OH radicals generated during the irradiation period, we turned off the illumination instantly and monitored the variation of EPR signals with time in the dark. As displayed in Fig. 6a, when illumination was switched off, the four peaks associated with DMPO–$^{\bullet}$OH adducts could still be distinguished for Se NR-1, but they were notably weaker than those under light illumination. After staying in the dark for 20 min, the EPR signals of Se NR-1 remained and continued to get depressed. For comparison purpose, we conducted the same measurement on P-25 TiO_2 powder and the result was shown in Fig. 6b. The quartet EPR signals again demonstrate the effective generation of $^{\bullet}$OH

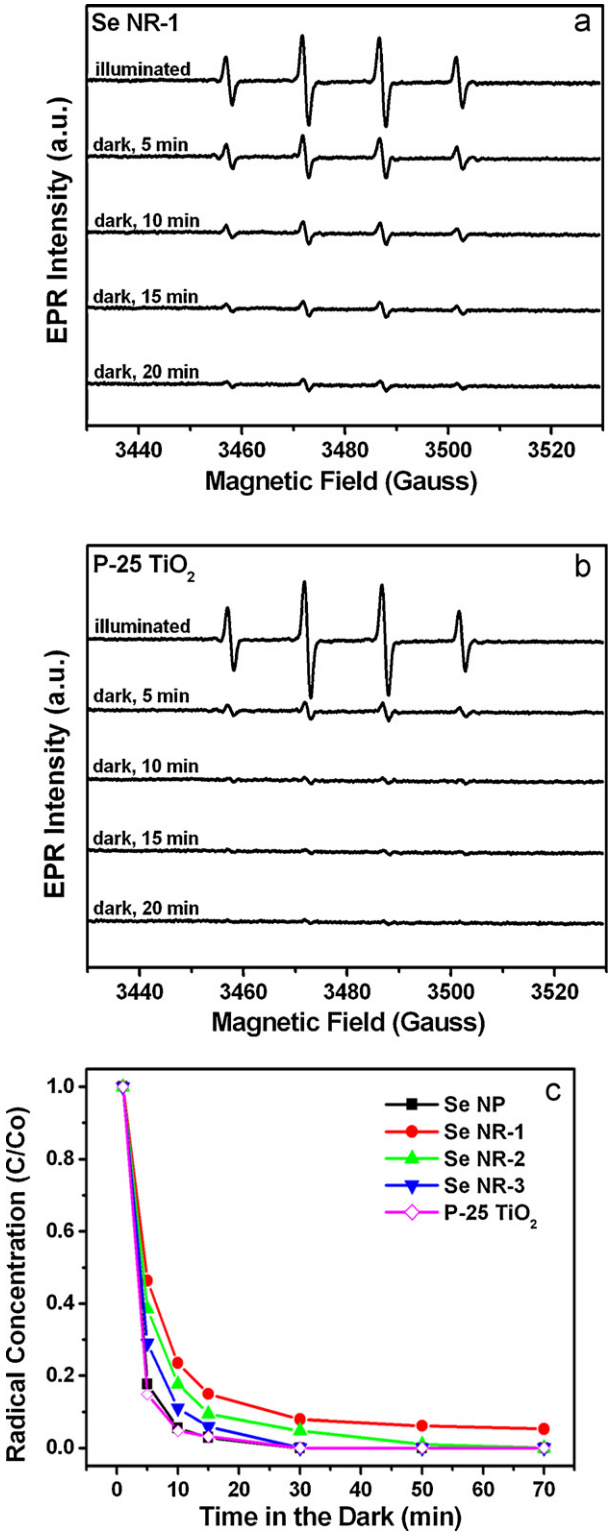

Fig. 6. Time evolution of DMPO–$^{\bullet}$OH EPR spectrum in the dark for (a) Se NR-1 and (b) P-25 TiO_2 samples. The variation of DMPO–$^{\bullet}$OH concentration with time in the dark for various samples was quantitatively compared in (c).

radicals for P-25 TiO_2 under light illumination. Besides, a faster decay of DMPO–•OH adducts was revealed for P-25 TiO_2 when compared with Se NR-1, which can be identified more clearly from the quantitative data presented in Fig. 6c. Also included in Fig. 6c were the DMPO–•OH decay results for Se nanoparticles and other Se NR samples. Interestingly, all the Se NR samples tested exhibited slower decay kinetics of DMPO–•OH adducts than P-25 TiO_2 and Se nanoparticles did. The pronounced capability for Se NRs to generate •OH in the dark may account for the long-lasting DMPO–•OH EPR signals as observed. Note that the decay process of DMPO–•OH adducts in the dark involves two serial reaction steps, the formation of DMPO–•OH by trapping •OH with DMPO and the degradation of DMPO–•OH by radical–radical termination [62]. As the EPR data in Fig. 6 were collected under identical experimental conditions, the difference in DMPO–•OH decay kinetics among samples should arise from the varied amounts of •OH that could be possibly generated. It should be mentioned that under light illumination of a fixed period, no significant difference in the intensity of DMPO–•OH EPR signals was found among Se NRs, Se nanoparticles and P-25 TiO_2, indicating a comparable production rate of •OH for all the irradiated samples. However, when irradiation was interrupted, production of •OH varied from sample to sample and was dominated by the charge carriers remaining at the surfaces of samples. For the present Se NRs under light illumination, abundant photogenerated charge carriers were believed to exist and transfer to their surfaces for participation in •OH production. Upon the cease of irradiation, charge carriers of considerable amount may still remain, offering additional supply of •OH in the dark to moderate the decay kinetics of DMPO–•OH. Consequently, relatively slow decay of DMPO–•OH adducts was observed for all the NR samples tested. The above supposition can be further validated by the memory photocatalytic effect demonstrated for Se NRs in dark environment, as will be discussed later.

3.5. Photocatalytic properties

To investigate the potential as a photocatalyst for the present Se NRs, we performed a series of photocatalysis experiments. MB, a typical dye for photodegradation, was used as the test pollutant to monitor the photocatalysis progress for the samples. Five kinds of photocatalysts including three Se NR samples (Se NR-1, Se NR-2, Se NR-3), Se nanoparticles (Se NP), and commercial P-25 TiO_2 powder were used for MB photodegradation under the same experimental conditions. The comparative results were shown in Fig. 7a, from which several points can be observed. First, experiment in the absence of photocatalyst showed slight degradation of MB, implying a minor extent of self-photolysis for MB molecules under UV illumination [63,64]. Second, the photocatalytic efficiency of Se NRs was depressed with increasing amount of NaOH employed, probably resulting from the lower specific surface area expected for longer NRs. As the length of NRs increased, the number of the surfaces comprising the tip and end of NR per unit weight of sample decreased, resulting in a reduction of the specific surface area for NRs. The BET surface area of Se NR-1, Se NR-2 and Se NR-3 was measured to be 46.6, 27.9, and 14.3 m^2/g, respectively. Such drastic decrease in specific surface area of NRs may substantially reduce the number of active sites for photocatalysis, which further led to the depression in the resulting photocatalytic efficiency as observed [65,66]. Third, as compared to the commercial P-25 TiO_2 powder and Se nanoparticles which had substantially large surface areas (54.8 and 53.2 m^2/g, respectively), the three Se NR samples all exhibited superior photocatalytic performance. This outcome was ascribed to the single crystallinity of NR structures that can facilitate the interior charge carrier transfer and thus improve the carrier utilization efficiency [67,68]. Similar result was ever reported for TiO_2 case, in which nanorods surpassed nanospheres in photocatalytic activity due to the enhanced interfacial charge transfer rate [69]. In addition, the intrinsically suppressed electron-hole recombination event expected for Se may also answer for the superb photocatalytic efficiency of the present Se NRs. The photocatalytic performance of the five photocatalysts was further examined after light exposure. In this experiment, sample was first irradiated for

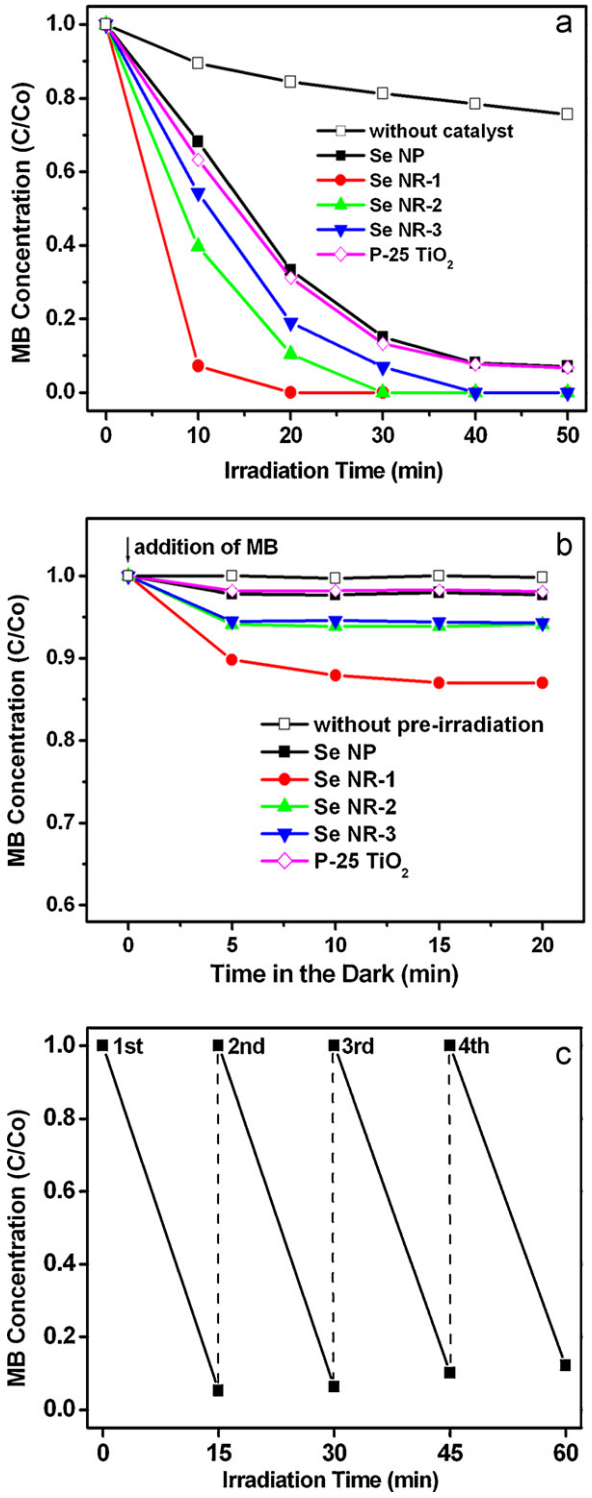

Fig. 7. (a) C/Co versus irradiation time plots for MB photodegradation without any catalyst and in the presence of various samples. (b) Results of MB degradation in the dark by using various samples subjected to a pre-irradiation of 5 min. The result for Se NR-1 sample without pre-irradiation treatment was also included for comparison. (c) Recycling test on Se NR-1 sample for MB photodegradation.

5 min to produce charge carries of sufficient amount. The illumination was then turned off, and MB degradation was conducted with the same experimental setup as the photocatalysis experiment described above except for the light illumination. Besides, in order to exclude the contribution of self-photolysis of dye molecules, MB was added into the photoreactor upon the cease of irradiation. The results of performance evaluation in dark environment for the five photocatalysts were compared in Fig. 7b. It was found that with the pre-irradiation of 5 min, both P-25 TiO_2 and Se nanoparticles showed considerably tiny effect toward MB degradation This result can be rationalized by the fact that only few charge carriers could remain at their surfaces to participate in •OH production and the subsequent MB degradation after the cease of irradiation. The observation of the fast decay kinetics of DMPO–•OH for P-25 TiO_2 and Se nanoparticles was in accordance with the above consequence. In contrast to P-25 TiO_2 and Se nanoparticles, the three pre-irradiated Se NR samples displayed rather noticeable photocatalytic activities in the dark. For Se NR-1 sample, the catalytic effect toward MB degradation persisted even after 20 min in dark environment. The sustained supply of •OH in the dark for Se NRs, which was inferred from their relatively slow decay kinetics of DMPO–•OH, may account for the memory photocatalytic effect as observed. To substantiate such memory photocatalytic effect, we conducted a comparative experiment by applying Se NR-1 in MB degradation without prior illumination. Apparently, no degradation of MB could be attained in the dark if Se NR-1 was not subjected to pre-irradiation. This demonstration reaffirms that the capability of photocatalysis in dark environment for Se NRs resulted from the memory effect related to pre-irradiation treatment. To further demonstrate the remarkable photocatalytic properties for Se NRs, a recycling test by using Se NR-1 as the representative photocatalyst was performed. As shown in Fig. 7c, no appreciable decay of photocatalytic activity was found for Se NRs after they were repeatedly used and recycled in MB photodegradation for four times. This result reveals that the present Se NRs could be promisingly utilized in the long-term course of photocatalysis.

4. Conclusions

In conclusion, we have successfully developed a facile CMC-stabilized chemical reduction approach for preparation of single-crystalline Se NRs at room temperature. The growth of Se NRs involved the reduction of H_2SeO_3 with $NaBH_4$ to form Se particle seeds, followed by the anisotropic growth of Se directed by CMC molecules and the subsequent crystal growth along a preferred direction from these seeds to form NRs. Through suitably modulating the reaction conditions such as the reaction temperature and the amount of NaOH added, the dimensions of the resulting Se NRs can be readily controlled. Spin-trapping EPR analysis suggests that a sustained supply of •OH radicals could be attained for Se NRs upon the cease of irradiation. With the capability of •OH production in the dark, Se NRs were found for the first time to display noticeable photocatalytic activities in dark environment after subjected to a short period of irradiation. As compared to the commercial P-25 TiO_2 and Se nanoparticles, the as-synthesized Se NRs exhibited superior photocatalytic performance toward MB photodegradation, attributable to the single crystallinity of NR structures that can facilitate the interior charge carrier transfer and thus improve the carrier utilization efficiency. In addition, the intrinsically suppressed electron-hole recombination event expected for Se may answer for the superb photocatalytic efficiency of the present Se NRs as well. Furthermore, Se NRs retained comparable photocatalytic activity after repeated uses and recycled, revealing that they could be promisingly utilized in the long-term course of photocatalysis. The present Se NRs may find potential use for unique photocatalytic applications, in which typical photocatalysis prevails under light illumination, while memory photocatalytic effect takes over when irradiation is interrupted. The current study also gives rise to a new type of photocatalysts that can effectively produce chemical energy from absorbing light in a new-fashioned way.

Acknowledgments

This work was financially supported by the National Science Council of the Republic of China (Taiwan) under grant NSC-98-2213-M-009-015-MY2, and by National Chiao Tung University under grant 99W963.

References

[1] H.T. Li, P.J. Regensburger, J. Appl. Phys. 34 (1963) 1730–1734.
[2] J.A. Johnson, M.L. Saboungi, P. Thiyagarajan, R. Csencsits, D. Meisel, J. Phys. Chem. B 103 (1999) 59–63.
[3] B. Gates, B. Mayers, B. Cattle, Y.N. Xia, Adv. Funct. Mater. 12 (2002) 219–227.
[4] K. Mondal, P. Roy, S.K. Srivastava, Cryst. Growth Des. 8 (2008) 1580–1584.
[5] B. Gates, Y.Y. Wu, Y.D. Yin, P.D. Yang, Y.N. Xia, J. Am. Chem. Soc. 123 (2001) 11500–11501.
[6] B. Gates, B. Mayers, Y.Y. Wu, Y.G. Sun, B. Cattle, P.D. Yang, Y.N. Xia, Adv. Funct. Mater. 12 (2002) 679–686.
[7] U. Jeong, Y. Xia, Angew. Chem. Int. Ed. 44 (2005) 3099–3103.
[8] G.D. Moon, U. Jeong, Langmuir 25 (2009) 458–465.
[9] R.Z. Ma, Y. Wang, T.E. Mallouk, Small 5 (5) (2009) 356–360.
[10] X.C. Jiang, B. Mayers, T. Herricks, Y.N. Xia, Adv. Mater. 15 (2003) 1740–1743.
[11] G.Q. Zhang, W. Wang, Q.X. Yu, X.G. Li, Chem. Mater. 21 (2009) 969–974.
[12] X.C. Jiang, B. Mayers, Y.L. Wang, B. Cattle, Y.N. Xia, Chem. Phys. Lett. 385 (2004) 472–476.
[13] C.X. Fang, S.Y. Zhang, P.G. Zuo, W. Wei, B.K. Jin, J.Y. Wu, Y.P. Tian, J. Cryst. Growth 311 (2009) 2345–2351.
[14] B. Mayers, X. Jiang, D. Sunderland, B. Cattle, Y.N. Xia, J. Am. Chem. Soc. 125 (2003) 13364–13365.
[15] G.D. Moon, U. Jeong, Chem. Mater. 20 (2008) 3003–3007.
[16] C.J. Murphy, A.M. Gole, S.E. Hunyadi, J.W. Stone, P.N. Sisco, A. Alkilany, B.E. Kinard, P. Hankins, Chem. Commun. (2008) 544–557.
[17] Y.G. Sun, J.Q. Hu, Z.G. Chen, Y.S. Bando, D. Golberg, J. Mater. Chem. 19 (2009) 7592–7605.
[18] T.Y. Zhai, X.S. Fang, L. Li, Y.S. Bando, D. Golberg, Nanoscale 2 (2010) 168–187.
[19] A.I. Hochbaum, P.D. Yang, Chem. Rev. 110 (2010) 527–546.
[20] B. Gates, B. Mayers, A. Grossman, Y.N. Xia, Adv. Mater. 14 (2002) 1749–1752.
[21] B. Mayers, K. Liu, D. Sunderland, Y.N. Xia, Chem. Mater. 15 (2003) 3852–3858.
[22] H. Zhang, D.R. Yang, Y.J. Ji, X.G. Ma, J. Xu, D.L. Que, J. Phys. Chem. B 108 (2004) 1179–1182.
[23] X.M. Li, Y. Li, S.Q. Li, W.W. Zhou, H.B. Chu, W. Chen, I.L. Li, Z.K. Tang, Cryst. Growth Des. 5 (2005) 911–916.
[24] Z.X. Chen, Y.H. Shen, A.J. Xie, J.M. Zhu, Z.F. Wu, F.Z. Huang, Cryst. Growth Des. 9 (2009) 1327–1333.
[25] B. Gates, Y.D. Yin, Y.N. Xia, J. Am. Chem. Soc. 122 (2000) 12582–12583.
[26] A. Abdelouas, W.L. Gong, W. Lutze, J.A. Shelnutt, R. Franco, I. Moura, Chem. Mater. 12 (2000) 1510–1512.
[27] X.Y. Gao, T. Gao, L.D. Zhanga, J. Mater. Chem. 13 (2003) 6–8.
[28] Z.W. Quan, P.P. Yang, C.X. Li, X.M. Zhang, J. Yang, J. Lin, Cryst. Growth Des. 8 (2008) 3834–3839.
[29] S. Ko, M. Park, J.S. Lee, Y.S. Kim, D.Y. Ryu, U. Jeong, Chem. Commun. (2009) 1855–1857.
[30] X.Y. Liu, M.S. Mo, J.H. Zeng, Y.T. Qian, J. Cryst. Growth 259 (2003) 144–148.
[31] Z.H. Wang, X.Y. Chen, J.W. Liu, X.G. Yang, Y.T. Qian, Inorg. Chem. Commun. 6 (2003) 1329–1331.
[32] C.H. An, K.B. Tang, X.M. Liu, Y.T. Qian, Eur. J. Inorg. Chem. (2003) 3250–3255.
[33] B. Zhang, W. Dai, X.C. Ye, F. Zuo, Y. Xie, Angew. Chem. Int. Ed. 45 (2006) 2571–2574.
[34] Y.R. Ma, L.M. Qi, J.M. Ma, H.M. Cheng, Adv. Mater. 16 (2004) 1023–1026.
[35] M.B. Yim, P.B. Chock, E.R. Stadtman, Proc. Natl. Acad. Sci. U.S.A. 87 (1990) 5006–5010.
[36] V. Krishna, D. Yanes, W. Imaram, A. Angerhofer, B. Koopman, B. Moudgil, Appl. Catal. B: Environ. 79 (2008) 376–381.
[37] G. Brunton, D. Forrest, D. Griller, K.U. Ingold, A.H. Reddoch, J. Am. Chem. Soc. 100 (1978) 3721–3723.
[38] N.H. Chou, X.L. Ke, P. Schiffer, R. Schaak, J. Am. Chem. Soc. 130 (2008) 8140–8141.
[39] N. Geoffroy, G.P. Demopoulos, Ind. Eng. Chem. Res. 48 (2009) 10240–10246.
[40] J.M. Song, Y.J. Zhan, A.W. Xu, S.H. Yu, Langmuir 23 (2007) 7321–7327.
[41] J. Zhang, F.X. Wang, Z.W. Liu, S.T. Zhang, Y.Y. Zhang, J.Y. Liang, Y.P. Wang, Nat. Prod. Res. 23 (2009) 1641–1651.
[42] S. Magdassi, A. Bassa, Y. Vinetsky, A. Kamyshny, Chem. Mater. 15 (2003) 2208–2217.
[43] J.C. Liu, J. Sutton, C.B. Roberts, J. Phys. Chem. C 111 (2007) 11566–11576.
[44] J.C. Liu, F. He, E. Durham, D.G. Zhao, C.B. Roberts, Langmuir 24 (2008) 328–336.

[45] F. He, J.C. Liu, C.B. Roberts, D.G. Zhao, Ind. Eng. Chem. Res. 48 (2009) 6550–6557.
[46] J.C. Liu, F. He, T.M. Gunn, D.G. Zhao, C.B. Roberts, Langmuir 25 (2009) 7116–7128.
[47] F. He, D.G. Zhao, J.C. Liu, C.B. Roberts, Ind. Eng. Chem. Res. 46 (2007) 29–34.
[48] A.B. Bourlinos, I. Panagiotopoulos, D. Niarchos, D. Petridis, J. Mater. Res. 19 (2004) 1227–1233.
[49] B. Zhang, W.Y. Hou, X. Zhu, X.C. Ye, L.F. Fei, X.M. Liu, J.L. Yang, Y. Xie, Small 3 (2007) 101–105.
[50] X.H. Yang, W.L. Zhu, Cellulose 14 (2007) 409–417.
[51] L.H. Dong, Y. Chu, Y.J. Zhuo, W. Zhang, Nanotechnology 20 (2009) 125301.
[52] J. Lu, X.L. Jiao, D.R. Chen, W. Li, J. Phys. Chem. C 113 (2009) 4012–4017.
[53] C. Tsang, S.Y. Lai, A. Manthiram, Inorg. Chem. 36 (1997) 2206–2210.
[54] C.F. Tsang, J.K. Kim, A. Manthiram, J. Mater. Chem. 8 (1998) 425–428.
[55] F. Kim, K. Sohn, J.S. Wu, J.X. Huang, J. Am. Chem. Soc. 130 (2008) 14442–14443.
[56] K. Pal, A.K. Banthia, D.K. Majumdar, Trends Biomater. Artif. Organs 19 (2005) 12–14.
[57] M.J. O'Neil, The Merck Index, 13th ed., 2001, p. 308.
[58] M.A. Gilleo, J. Chem. Phys. 19 (1951) 1291–1297.
[59] P. Liu, Y.R. Ma, W.W. Cai, Z.Z. Wang, J. Wang, L.M. Qi, D.M. Chen, Nanotechnology 18 (2007) 205704.
[60] A. Qin, Z. Li, R. Yang, Y. Gu, Y. Liu, Z.L. Wang, Solid State Commun. 148 (2008) 145–147.
[61] T. Wu, T. Lin, J. Zhao, H. Hidaka, N. Serpone, Environ. Sci. Technol. 33 (1999) 1379–1387.
[62] K.P. Madden, H. Taniguchi, Free Radical Biol. Med. 30 (2001) 1374–1380.
[63] A. Houas, H. Lachheb, M. Ksibi, E. Elaloui, C. Guillar, J.M. Herrmann, Appl. Catal. B: Environ. 31 (2001) 145–157.
[64] K.L. Zhang, X.P. Lin, F.Q. Huang, W.D. Wang, J. Mol. Catal. A: Chem. 258 (2006) 185–190.
[65] X.L. Hu, G.S. Li, J.C. Yu, Langmuir 26 (2010) 3031–3039.
[66] F. Amano, K. Nogami, M. Tanaka, B. Ohtani, Langmuir 26 (2010) 7174–7180.
[67] H.S. Jung, Y.J. Hong, Y.R. Li, J.G. Cho, Y.J. Kim, G.C. Yi, ACS Nano 2 (2008) 637–642.
[68] Y.-C. Pu, Y.-C. Chen, Y.-J. Hsu, Appl. Catal. B: Environ. 97 (2010) 389–397.
[69] H.J. Yun, H. Lee, J.B. Joo, W. Kim, J. Yi, J. Phys. Chem. C 113 (2009) 3050–3055.